The Journal of Experimental Biology 211, 3214-3225
Published by The Company of Biologists 2008
doi:10.1242/jeb.020677

The influence of oxygen and high-energy phosphate diffusion on metabolic scaling in three species of tail-flipping crustaceans

Ana Gabriela Jimenez[1,*], Bruce R. Locke[2] and Stephen T. Kinsey[1]

[1]Department of Biology and Marine Biology, University of North Carolina Wilmington, 601 South College Road, Wilmington, NC 28403-5915, USA and [2]Department of Chemical and Biomedical Engineering, Florida State University, FAMU-FSU College of Engineering, Tallahassee, FL 32310-6046, USA

*Author for correspondence (e-mail: agj6818@uncw.edu)

Accepted 21 July 2008

SUMMARY

We examined the influence of intracellular diffusion of O_2 and high-energy phosphate (HEP) molecules on the scaling with body mass of the post-exercise whole-animal rate of O_2 consumption ($\dot{V}_{O_2}$) and muscle arginine phosphate (AP) resynthesis rate, as well as muscle citrate synthase (CS) activity, in three groups of tail-flipping crustaceans. Two size classes in each of three taxa (*Palaemonetes pugio*, *Penaeus* spp. and *Panulirus argus*) were examined that together encompassed a 27,000-fold range in mean body mass. In all species, muscle fiber size increased with body mass and ranged in diameter from 70±1.5 to 210±8.8 μm. Thus, intracellular diffusive path lengths for O_2 and HEP molecules were greater in larger animals. The body mass scaling exponent, *b*, for post-tail flipping $\dot{V}_{O_2}$ (*b*=–0.21) was not similar to that for the initial rate of AP resynthesis (*b*=–0.12), which in turn was different from that of CS activity (*b*=0.09). We developed a mathematical reaction–diffusion model that allowed an examination of the influence of O_2 and HEP diffusion on the observed rate of aerobic flux in muscle. These analyses revealed that diffusion limitation was minimal under most conditions, suggesting that diffusion might act on the evolution of fiber design but usually does not directly limit aerobic flux. However, both within and between species, fibers were more diffusion limited as they grew larger, particularly when hemolymph P_{O_2} was low, which might explain some of the divergence in the scaling exponents of muscle aerobic capacity and muscle aerobic flux.

Key words: oxygen consumption, arginine phosphate, citrate synthase activity, aerobic metabolism, anaerobic metabolism, metabolic scaling, diffusion.

INTRODUCTION

Predator–prey interactions result in strong selection for efficient escape responses in prey, and in some crustaceans a tail-flip response provides this vital function. Tail-flipping consists of fast backward propulsion resulting from the contraction of the abdominal musculature in response to a predator attack or other external stimuli. The anaerobic fibers that power tail-flipping in some species of crustaceans are often among the largest cells in the animal kingdom. Mammalian muscle cells typically range from approximately 10 to much less than 100 μm in diameter (Russell et al., 2000). This fundamental design constraint yields a high fiber-surface-area to volume ratio (SA:V) and short intracellular diffusion distances. Exceeding this maximum size might therefore compromise aerobic metabolism, which relies on oxygen flux from the blood to the mitochondria and ATP-equivalent diffusion within the cytoplasm (Mainwood and Rakusan, 1982; Meyer, 1988; Hubley et al., 1997; Boyle et al., 2003; Johnson et al., 2004; Kinsey et al., 2005; Hardy et al., 2006). However, some crustacean anaerobic fibers can be hundreds of microns in diameter (Hoyle et al., 1973; Kinsey and Ellington, 1996; Boyle et al., 2003). Furthermore, muscle growth in crustaceans largely occurs hypertrophically – that is, muscle mass increases owing to an increase in fiber diameter and length, whereas fiber number remains nearly constant (Bittner and Traut, 1978; Boyle et al., 2003). As some species of crustaceans undergo an extreme increase in body mass during development, there is a parallel increase in muscle fiber size. Thus, crustacean muscle fibers from juveniles fall within the fiber size range typical of many animals, but, as the animals grow, the fibers can greatly exceed the usual threshold on cellular dimensions, while still preserving function (Boyle et al., 2003; Johnson et al., 2004).

During tail-flipping, energy requirements exceed aerobic capacity and contraction is anaerobic and therefore is not constrained by diffusion of O_2 to mitochondria or ATP from mitochondria (England and Baldwin, 1983). Following bursts of tail-flipping, recovery must occur before the animal can generate another round of high-force contractions. Metabolism during an anaerobic burst–escape response in crustacean muscle follows the same pattern as in vertebrates. Contraction is initially powered by the hydrolysis of the phosphagen arginine phosphate (AP), which is the crustacean analog of phosphocreatine (PCr) in vertebrates. Once AP pools are nearly depleted, ATP for additional contractions is supplied by anaerobic glycogenolysis, which is reflected by the accumulation of lactate and depletion of glycogen (England and Baldwin, 1983; Booth and McMahon, 1985; Head and Baldwin, 1986; Milligan et al., 1989; Morris and Adamczewska, 2002). These glycogenolytically powered contractions are slower and less forceful than those powered by phosphagen hydrolysis (England and Baldwin, 1983; Head and Baldwin, 1986; Baldwin et al., 1999; Boyle et al., 2003).

In contrast to burst contraction, metabolic recovery *following* contraction in crustaceans does not always follow the vertebrate paradigm. Vertebrates rely exclusively on aerobic metabolism to power resynthesis of creatine phosphate, and lactate does not accumulate following contraction (Kushmerick, 1983; Meyer, 1988; Curtin et al., 1997), whereas it is widely known that crustaceans

often produce lactate after contraction (i.e. Head and Baldwin, 1986; Henry et al., 1994). In addition, Johnson and colleagues (Johnson et al., 2004) found that post-contractile lactate accumulation was fiber size dependent in blue crabs, in which large fibers produced significant amounts of lactate after contraction, whereas small crabs had no significant increase. These findings are consistent with those of Boyle and colleagues (Boyle et al., 2003), who reported significant post-contractile depletion of glycogen in aerobic fibers from large, but not small, crabs. Presumably, adult crabs are exploiting anaerobic metabolism to accelerate certain key phases of recovery such as AP resynthesis, the rate of which would otherwise be restricted by large fiber size (Kinsey and Moerland, 2002; Boyle et al., 2003; Johnson et al., 2004; Kinsey et al., 2005). It also has been suggested that, as animal size increases, the negative allometry of aerobic metabolism would place heightened demands on anaerobic glycogenolysis during recovery (Baldwin et al., 1999). As anaerobic metabolism utilizes endogenous substrates and does not require oxygen, the scope of metabolic energy expenditure becomes limited only by maximal enzyme activity (Wells et al., 2001). Thus, anaerobic glycogenolysis is not limited by diffusive constraints, making it an effective means of accelerating AP resynthesis in large fibers. However, reliance on anaerobic glycogen to speed recovery will put the animal further in oxygen debt, and complete recovery must ultimately be aerobic.

The fiber-size dependence of metabolic recovery described above is consistent with intracellular diffusion limitation. However, previous studies using reaction–diffusion models suggest that the intracellular diffusive flux of high-energy phosphate (HEP) molecules and associated metabolites (ATP, ADP, P_i, AP/PCr and arginine/creatine) does not lead to sizable intracellular concentration gradients in the very large anaerobic fibers of crustacean or fish muscle, despite the fact that diffusion might occur over hundreds of microns (Kinsey et al., 2005; Hardy et al., 2006; Nyack et al., 2007). It should be noted, however, that many fibers in adult animals appear to be as large as possible without encountering severe diffusion limitations (Kinsey at al., 2007). The absence of strong concentration gradients in HEP molecules suggests that low fiber SA:V and limited O_2 flux might be a more important factor to consider when examining the rate of recovery in large fibers. Evidence supporting this argument includes previously observed shifts in the distribution of mitochondria towards the periphery of the fiber during growth of crustacean and fish white muscle, which might help counteract the low SA:V in the large fibers of adults (Boyle et al., 2003; Nyack et al., 2007). In addition, the open circulatory system present in crustaceans is associated with relatively low extracellular P_{O_2} (Forgue et al., 2001), which might lead to rates of O_2 delivery that are insufficient to fuel high aerobic fluxes (Raffin et al., 1988; Mente et al., 2003).

The results described above imply an effect of muscle fiber size on aerobic metabolism in the blue crab; however, it is not known whether these effects constitute a fundamental diffusion constraint on cell design that can be broadly observed. Furthermore, it is not clear whether concentration gradients within the fiber actually lead to an alteration of aerobic metabolic flux. In the current study, the objectives were to examine the relationship between the scaling with body mass of whole-animal metabolic rate (rate of O_2 consumption, or $\dot{V}_{O_2}$), as well as the scaling of muscle aerobic capacity (citrate synthase activity) and a muscle metabolic process (post-contractile AP resynthesis) in three groups of tail-flipping crustaceans: the grass shrimp (*Palaemonetes pugio*), brown and pink shrimp (*Penaeus* spp.) and the spiny lobster (*Panulirus argus*). These species differ dramatically in body mass range during development, which facilitates both an intraspecific and interspecific analysis of scaling. We analyzed the *observed* post-contractile muscle recovery rates by developing a mathematical reaction–diffusion model that accounts for both O_2 and HEP diffusive flux and allows the evaluation of the influence of diffusion on aerobic flux. This is an advance over previous models that considered only the magnitude of the concentration gradients. This approach allowed us to determine the extent to which diffusion limits aerobic metabolism in muscle and potentially alters scaling relationships.

MATERIALS AND METHODS

Animal care and maintenance

The current study used a small (juvenile) and large (adult) size class for each species. Grass shrimp (*P. pugio* Holthius) were collected from River Road Park in Wilmington, NC, USA, and brown shrimp (*P. aztecus* Ives) and pink shrimp (*P. duorarum* Burkenroad) were collected by trawl offshore of Masonboro Inlet, NC, USA or ordered from Gulf Specimens (Panacea, FL, USA). Brown shrimp and pink shrimp are morphologically and behaviorally similar, and we found no differences between species in any of the measurements that we made. Therefore, both species were pooled as *Penaeus* spp. Juvenile *P. argus* Latreille were ordered from the Keys Marine Laboratory, FL, USA, and adult *P. argus* were collected by SCUBA diving 40 miles offshore of Wilmington, NC, USA. Water temperatures during collection for all species were 20–25°C as animals from NC were collected during the summer months. All animals were maintained in tanks containing filtered sea water that was constantly aerated. Smaller animals were maintained in glass aquaria at 20–22°C and a 12 h:12 h L:D photoperiod. Larger animals were maintained in 635 litre fiber-glass aquaria under the same conditions. Temperature was monitored daily, and water quality (nitrates, nitrite, pH and ammonia) was monitored weekly using a Salt Water Master Kit (Aquarium Pharmaceuticals, Chalfont, PA, USA). All animals were held for at least 1 week before experimentation. They were fed every other day, although feeding was stopped 24 h before any of the oxygen consumption trials to prevent spuriously high metabolic rates due to digestive activities.

Whole-animal oxygen consumption

Closed-chamber respirometry was used to measure the standard and post-contractile mass-specific rate of oxygen consumption ($\dot{V}_{O_2}$). $\dot{V}_{O_2}$ was measured using a YSI Model 5300 dissolved oxygen meter (Yellow Springs, OH, USA), using chambers with capacities of 20, 425, 800, 4000, 8000 and 26,000 ml. Before running an oxygen-consumption trial, the dissolved-oxygen electrode was calibrated with air-saturated sea water to ensure 100% oxygen saturation. Animals were placed in the chamber and were left to acclimatize for an hour before measurements. All trials were conducted during daylight hours, and chambers were covered to avoid visual disturbances that might cause increases in standard metabolic rate. During the acclimatization time, the water was constantly air saturated to prevent any possible oxygen depletion. After acclimatization, the chamber was submerged in salt water to eliminate bubbles inside the chamber, and it was then promptly sealed. $\dot{V}_{O_2}$ was continuously recorded using a Servogor 102 chart recorder until O_2 in the chamber dropped to 70% air saturation. Following the measurement of standard metabolic rates, the animals were provoked to tail-flip a predetermined number of times. The number of tail-flips that led to exhaustion in each species was measured in pilot studies, and the numbers of tail-flips used for measurements of $\dot{V}_{O_2}$ were half of those previously measured as exhaustive work. Following the exercise protocol, the chamber was

again sealed, and post-contractile $\dot{V}_{O_2}$ was measured. Animals were allowed to consume 30% of the oxygen in the chamber before measurements were stopped.

Muscle fiber diameter

Tail muscle was excised, mounted using optimal cutting temperature (O.C.T.) compound (Sakura Finetek, Torrance, CA, USA) and allowed to equilibrate to –19°C in a Reichert–Jung/Leica cryocut 1800 (Depew, NY, USA) before sectioning. Sections were cut at 20 μm using the cryocut microtome, picked up on slides and air-dried at room temperature. Sections were incubated for 30 min in a 25 mg/ml solution of the lectin wheat-germ agglutinin, which binds to sugars on the surface of endothelial cells in vascular pathways. Slides were then rinsed in the appropriate saline solution (for lobsters, a solution containing 452 mmol l^{-1} NaCl, 15 mmol l^{-1} KCl, 18.9 mmol l^{-1} $CaCl_2$, 4 mmol l^{-1} $MgCl_2$, 2.8 mmol l^{-1} $MgSO_4$ pH 7.4 and, for shrimps, a solution containing 525 mmol l^{-1} NaCl, 13.3 mmol l^{-1} KCl, 12.4 mmol l^{-1} $CaCl_2$, 24.8 mmol l^{-1} $MgCl_2$ pH 7.4) for 60 min. Stained slides were examined with an Olympus BX-60 microscope (Center Valley, PA, USA), and images were recorded with a SPOT RT-KE camera. Polygons of fiber diameters were traced using Adobe Photoshop (version 7.0), and Image Pro Plus (version 6.0) was used to analyze fiber diameters. The average diameter of the polygon traces through the centroid was calculated in two-degree increments around the circumference of the cell.

Muscle citrate synthase activity

Citrate synthase (CS) activity assays were conducted based on the methods of Walsh and Henry (Walsh and Henry, 1990). Abdominal muscle was excised and freeze-clamped in liquid nitrogen and stored in plastic vials at –80°C until use. Tissue was extracted in 5–20 volumes of enzyme extraction buffer containing 50 mmol l^{-1} Tris, 1 mmol l^{-1} EDTA, 2 mmol l^{-1} $MgCl_2$, 2 mmol l^{-1} DTT at a pH of 7.6 and then sonicated on ice at 10 W in three bursts of 5 s each. Samples were centrifuged for 20 min at 16,000 ***g***, and the supernatant was combined with 1 mmol l^{-1} 5,5-dithio-bis (2-nitobenzoic acid), 0.3 mmol l^{-1} acetyl coenzyme A and water. Absorbance at a wavelength of 412 nm was measured in an Ultrospec 4000 spectrophotometer (Amersham-Pharmacia Biotech, Buckinghamshire, UK) at 25°C until the absorbance stabilized. The absorbance change during this period was slight and typically stabilized in 2–3 min. The reaction was initiated by the addition of 0.5 mmol l^{-1} oxaloacetate, and the enzyme activity was determined from the initial slope of the absorbance change.

Muscle arginine phosphate recovery rate

During a burst exercise–recovery cycle, there is a reciprocal change in AP and inorganic phosphate (P_i) that results from the stoichiometric coupling of cellular ATPases and the arginine kinase reaction. Contraction results in a rapid depletion of AP, and corresponding increase in P_i, which is followed by a slow recovery to pre-contractile levels, where the initial phase of recovery is the most rapid. To characterize the maximal rate of AP recovery, animals were exercised following the above protocol, and, after a pre-determined recovery period, the abdomen was rapidly removed by a swift cut between the abdomen and the cephalothorax. The first segment of the abdominal musculature was removed from the animal. The muscle was immediately freeze-clamped in liquid nitrogen. Tissues were immediately homogenized in a 5–60-fold dilution of chilled 7% perchloric acid with 1 mmol l^{-1} EDTA and then centrifuged at 16,000 ***g*** for 30 min at 4°C. The supernatant pH was neutralized with 3 mol/l potassium bicarbonate in 50 mmol l^{-1} PIPES, stored on ice for 10 min and centrifuged at 16,000 ***g*** for 15 min at 4°C. The supernatant was immediately analyzed by ^{31}P nuclear magnetic resonance (NMR) spectroscopy. NMR spectra were collected at 162 MHz on a Bruker 400 DMX spectrometer (Billerica, MA, USA) to determine the relative concentrations of AP, ATP and P_i. Spectra were collected using a 90° excitation pulse and a relaxation delay of 12 s, which ensured that the phosphorus nuclei were fully relaxed and peak integrals for the metabolites were proportional to their relative concentrations. The area under each peak was integrated using Xwin-NMR software to yield the relative concentrations of each metabolite, and these values were converted to concentration by assuming a total HEP concentration of 50 mmol l^{-1}, which is characteristic of crustacean white muscle (see Kinsey et al., 2005). The initial slope of AP recovery was essentially linear with time, and so we used linear regression to determine the maximal rate of AP resynthesis following contraction.

Muscle L-lactate concentration

Muscle lactate was measured immediately after exercise and following 15 min of recovery to estimate the fiber size dependence of post-contractile reliance on anaerobic metabolism. Frozen tissue samples were homogenized in 5–60-fold dilutions of chilled 7% perchloric acid with 1 mmol l^{-1} EDTA, and then centrifuged at 4°C at 16,000 ***g*** for 30 min. The supernatant was neutralized using 3 mol/l potassium bicarbonate in 50 mmol l^{-1} PIPES and centrifuged at 4°C at 16,000 ***g*** for 15 min. The resulting supernatant was stored at –80°C until use. The concentration of L-lactate in the tail musculature of crustaceans was spectrophotometrically assayed following the procedures of Lowry and Passonneau (Lowry and Passonneau, 1972), as modified by Kinsey and Ellington (Kinsey and Ellington, 1996). A buffer containing 300 mmol l^{-1} hydrazine hydrate, 12 mmol l^{-1} EDTA and 4 mmol l^{-1} NAD^+ at pH 9.0 was mixed with the tissue extract in a 0.5 ml cuvette, and absorbance was monitored at a wavelength of 340 nm to obtain a stable baseline. The reaction was initiated by the addition of 18.5 units of L-lactate dehydrogenase, and the change in absorbance was measured. The concentration in the sample was calculated by assuming that 1 g of muscle tissue has 0.75 ml of intracellular water (Milligan et al., 1989).

Statistical analysis

The influence of body mass on specific $\dot{V}_{O_2}$, CS activity and AP recovery were analyzed using linear regression analysis, and analysis of covariance (ANCOVA) was used to compare scaling relationships. Fiber diameter was compared between each size class within a species using Student's *t*-tests. Student's *t*-tests were also used to compare lactate concentration immediately after exercise with the concentration 15 min post exercise. Results were considered significant if $P<0.05$.

Reaction–diffusion model

The mathematical model was developed for the system shown in Fig. 1, where O_2 is supplied at a fixed blood stream concentration, C^o, and it is transported from the blood to the fiber through a barrier that represents the vascular endothelium and cell membrane with a fixed resistance, $1/k_{mt}$. O_2 is consumed by a pseudo-homogeneous second-order reaction at the mitochondria, with 6 moles of ADP forming 6 moles of ATP for every mole of O_2 by the overall reaction:

$$O_2 + 6ADP \rightarrow 6ATP \ . \quad (1)$$

The mitochondria are assumed to be uniformly distributed throughout the region from x=0 (boundary of cell next to vasculature) to x=L (center of cell), and the rate constant for this reaction reflects

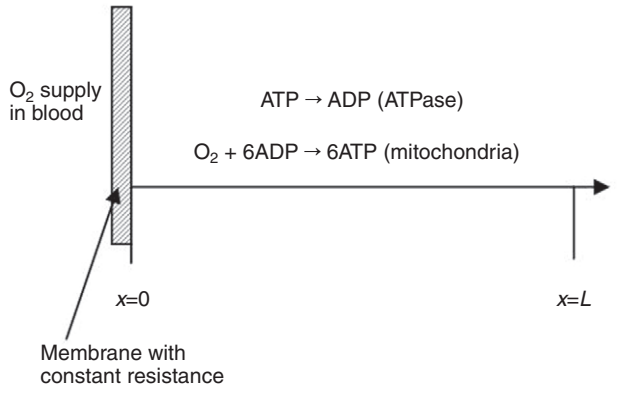

Fig. 1. Schematic of mathematical model showing one-dimensional spatial domain where the position in the cell, *x*, ranges from *x*=0 (sarcolemma) to *x*=*L* (fiber center). O_2 is supplied at a constant concentration on the outside of a membrane that constitutes the vascular endothelium, extracellular space and sarcolemma (hatched area), and the myosin ATPase and mitochondrial reactions are distributed uniformly through the spatial domain.

an averaged value accounting for the density of the mitochondria. The ATP formed by the mitochondria is consumed by a cellular ATPase by a first-order reaction:

$$\mathrm{ATP} \rightarrow \mathrm{ADP} + P_\mathrm{i} \,. \tag{2}$$

The ATPase is also assumed to be uniformly distributed through the domain from *x*=0 to *x*=L. The one-dimensional molar species balances for ADP, ATP and O_2, valid in the region from *x*=0 to *x*=L are given by:

$$\begin{aligned} D_{\mathrm{ATP}} \frac{d^2 c_{\mathrm{ATP}}}{dx^2} &= k_1 C_{\mathrm{ATP}} - k_2 C_{\mathrm{ADP}} C_{\mathrm{O_2}} \\ D_{\mathrm{O_2}} \frac{d^2 c_{\mathrm{O_2}}}{dx^2} &= (k_2 / 6) C_{\mathrm{ADP}} C_{\mathrm{O_2}} \\ C_{\mathrm{ATP}} + C_{\mathrm{ADP}} &= C_\mathrm{T} \,, \end{aligned} \tag{3}$$

where *D* is the diffusion coefficient, *C* is the concentration, k_1 is the rate constant governing the ATPase reaction, and k_2 is the rate constant for ATP production at the mitochondria. The boundary conditions for these equations are:

$$\begin{aligned} -D_{\mathrm{ATP}} \frac{dC_{\mathrm{ATP}}}{dx} &= 0 \qquad x = 0, L \\ -D_{\mathrm{O_2}} \frac{dC_{\mathrm{O_2}}}{dx} &= k_{\mathrm{mt}} \left(C^{\mathrm{o}} - C_{\mathrm{O_2}}(x=0) \right) \qquad x = 0 \\ -D_{\mathrm{O_2}} \frac{dC_{\mathrm{O_2}}}{dx} &= 0 \qquad x = L \,. \end{aligned} \tag{4}$$

The first boundary condition reflects the fact that ATP is not transported out of the cell and there is symmetry about the cell center (*x*=*L*). The second boundary condition describes the transport of oxygen across the vascular walls and cell membrane by diffusion with a linear driving force, where C^{o} is the bloodstream concentration of O_2. The last boundary condition indicates that the oxygen distribution is symmetric with respect to the center of the cell, as in the case for ATP in the first boundary condition. The above system of equations is solved using the boundary value differential equation solver 'bvp5c' in MATLAB version 7.5.0.342 (Mathworks, Lowell, MA, USA) to determine the spatially dependent concentrations and to determine the flux at the boundary, *x*=0, as well as the average concentrations of oxygen and ATP defined by:

$$\begin{aligned} \left\langle C_{\mathrm{O_2}} \right\rangle &= \frac{1}{L} \int_0^L C_{\mathrm{O_2}} \, dx \\ \left\langle C_{\mathrm{ATP}} \right\rangle &= \frac{1}{L} \int_0^L C_{\mathrm{ATP}} \, dx \,. \end{aligned} \tag{5}$$

The effectiveness factors are determined following methods discussed previously (Locke and Kinsey, 2008). The effectiveness factor is defined as the ratio of the rate of the reaction in the presence of diffusion to the rate of the reaction in the absence of diffusion. It therefore can range from 0 (complete limitation of reaction flux by diffusion) to 1 (no limitation by diffusion), and it is a useful tool for assessing the extent of diffusion limitation. In the absence of diffusion, Eqns 3 and 4 can be shown to give:

$$\begin{aligned} \Omega_1 C_{1\mathrm{wo}} &= (1 - C_{1\mathrm{wo}}) \, C_{2\mathrm{wo}} \\ \Omega_2 \, (1 - C_{2\mathrm{wo}}) &= C_{2\mathrm{wo}} \, (1 - C_{1\mathrm{wo}}) \end{aligned} \tag{6}$$

where:

$$\begin{aligned} \Omega_1 &= \phi_1^{\,2} / \phi_2^{\,2} \\ \Omega_2 &= 6\gamma / (\phi_2^{\,2} D_\mathrm{R} C_\mathrm{R}) \\ \phi_1^{\,2} &= (k_1 L^2 / D_{\mathrm{ATP}}) \\ \phi_2^{\,2} &= (k_2 L^2 C^{\mathrm{o}} / D_{\mathrm{ATP}}) \\ D_\mathrm{R} &= D_{\mathrm{ATP}} / D_{\mathrm{O_2}} \\ C_\mathrm{R} &= C_\mathrm{T} / C_\mathrm{O} \\ C_{1\mathrm{wo}} &= C_{\mathrm{ATP}} / C_\mathrm{T} \\ C_{2\mathrm{wo}} &= C_{\mathrm{O_2}} / C^{\mathrm{o}} \,. \end{aligned} \tag{7}$$

Eqn 6 leads to a quadratic equation that can be solved easily for the non-dimensional ATP and oxygen concentrations in the absence of diffusion, $C_{1\mathrm{wo}}$ and $C_{2\mathrm{wo}}$, respectively. All roots of the quadratic are real; however, only one root is within the physical domain of the problem. The reaction rates in the case without and with diffusion, respectively, are determined from:

$$R_{\mathrm{wo}} = k_1 C_\mathrm{T} \, (C_{1\mathrm{wo}}) 60 \times 10^{15} \,. \tag{8}$$

$$r = (D_{\mathrm{ATP}} C_\mathrm{T} / L^2) \left[\frac{1}{D_\mathrm{R} C_\mathrm{R}} \left(-\frac{dC_2}{ds} \right)_{s=0} \right] 60 \times 10^{15} \,, \tag{9}$$

where the units of k_1 are in s^{-1}, those for C_T are $\mathrm{mmol\,\mu m^{-3}}$ and the rate is given in $\mathrm{mmol\,l^{-1}\,min^{-1}}$. In all calculations for this paper, the following parameters are fixed: D_{ATP}=70 $\mu\mathrm{m^2\,s^{-1}}$, $D_{\mathrm{O_2}}$=1160 $\mu\mathrm{m^2\,s^{-1}}$, C_T=10^{-14} $\mathrm{mmol\,\mu m^{-3}}$ and k_{mt}=1100 $\mu\mathrm{m\,s^{-1}}$

The concentration of oxygen at the source is either 2.50 $\mu\mathrm{mol\,l^{-1}}$ (low), 7.85 $\mu\mathrm{mol\,l^{-1}}$ (intermediate) or 35.33 $\mu\mathrm{mol\,l^{-1}}$ (high), where the latter two cases are based on experimental measurements in crustaceans (Forgue et al., 2001).

The effectiveness factor (η), which again is the ratio of the rate of reaction with diffusion to that in the absence of diffusion, is determined by the ratio of Eqn 9 to Eqn 8 and can be represented by:

$$\eta = \frac{1}{\phi_1^2 D_R C_R C_{1wo}} \left(-\frac{dC_2}{ds} \right) \Bigg|_{x=0} \qquad (10)$$
$$s = x / L$$
$$C_2 = C_{O_2} / C^o \ .$$

The gradient term in Eqns 9 and 10 is determined by the numerical solution of Eqn 3 and boundary conditions 4 in MATLAB.

The first set of calculations was determined using Eqn 6 to find the concentrations in the absence of diffusion for various values of k_1 and k_2. The resulting rates were determined by Eqn 8. In the absence of diffusion, it was found that multiple values of k_1 and k_2 could satisfy the reaction rate; however, there were minimal values of k_1 below which the rate could not be attained. Similar analysis was conducted in the case with diffusion to determine the rate using the numerical solution of Eqn 3 and evaluating the rate with Eqn 9. As in the no-diffusion case, it was found that a range of combinations of k_1 and k_2 can give the same reaction rate; therefore, another set of calculations for the cases in the presence of diffusion was performed to determine the value of k_2 for various fixed values of k_1 that would match the experimentally determined reaction rate. In this set of computations, the value of k_1 was set at fixed values of the smallest value that would satisfy the rate. For each k_1 value, a root-finding method was used to determine the value of k_2 that would give the desired experimental rate. The average concentrations of oxygen and ATP were determined in each of these cases (with fixed rate) by using Eqn 5. As a range of k_1 and k_2 can satisfy the rate, it is important to note that the average ATP and oxygen concentrations change – that is, the average ATP concentration – drops with increasing k_1.

RESULTS

Body mass

Grass shrimps ranged in body mass from 0.045 to 0.624 g, with mean body masses for the small and large size classes of 0.11±0.006 and 0.40±0.017 g, respectively; penaeid shrimps ranged from 0.96 to 25.3 g, with means for the small and large size classes of 3.7±0.223 and 10.5±0.466 g, respectively; and lobsters ranged from 70.4 to 3105 g, with means for the small and large size classes of 151.7±5.33 and 2950±35.6 g, respectively. This corresponded to a 69,000-fold body mass range across all species and a nearly 27,000-fold range in mean body mass across all species size classes.

Whole-animal oxygen consumption

The allometric scaling equation, $y=aM^b$, was used to evaluate aerobic metabolism as a function of body mass, where y is the measured physiological property, M is body mass, a is a constant, and b is the scaling exponent (Schmidt-Nielsen, 1984). Mass-specific metabolic rate was lower in larger animals, as expected, and post-exercise $\dot{V}_{O_2}$ was 2.4- to 3.2-fold higher than standard $\dot{V}_{O_2}$. Standard specific $\dot{V}_{O_2}$ had a body mass scaling exponent (b) of –0.18, and post-exercise specific $\dot{V}_{O_2}$ had a scaling exponent of –0.21 (Fig. 2). The fold increase in $\dot{V}_{O_2}$ due to exercise was also body mass specific, being greater in smaller animals. However, ANCOVA indicated that there was not a significant difference in the slope of the body mass dependence of standard and post-tail flip $\dot{V}_{O_2}$ (F=0.46, P=0.50).

Muscle fiber size

Fig. 3 illustrates the hypertrophic growth exhibited by the white abdominal musculature of the three species of crustaceans leading to larger fiber sizes in adults. Fiber size was proportional to body mass within and across species. Fibers in small *P. pugio* ranged from 35.6 to 130.9 µm, in large *P. pugio* from 47.3 to 150.3 µm, in small *Penaeus* spp. from 49.8 to 169.1 µm, in large *Penaeus* spp. from 31.7 to 258.1 µm and finally in small *P. argus* from 81.0 to 347.1 µm and in large *P. argus* from 18.6 to 317.2 µm. A Student's t-test indicated that, within each species, mean fiber sizes of small and large size classes were significantly different (Fig. 3, inset).

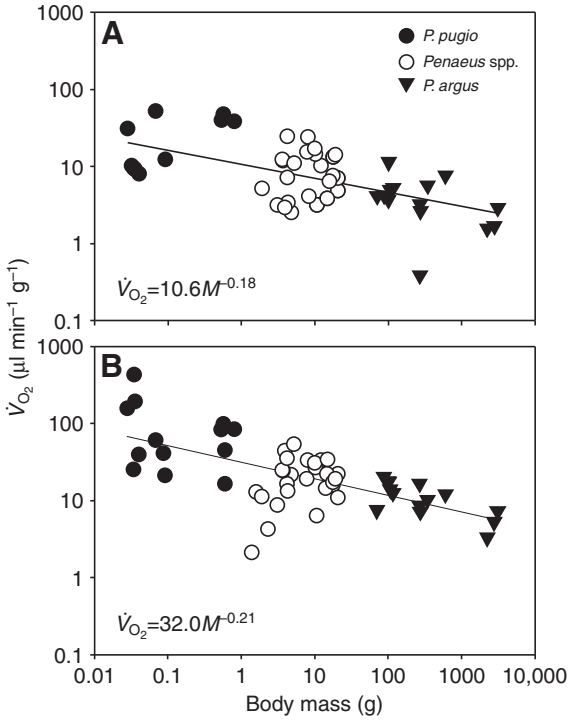

Fig. 2. (A) Standard and (B) post-exercise $\dot{V}_{O_2}$ for all three species and size classes. The scaling exponent, b, was –0.18 for standard $\dot{V}_{O_2}$ and –0.21 for post-exercise $\dot{V}_{O_2}$ (r^2=0.33 and 0.47, for standard $\dot{V}_{O_2}$ and post-exercise $\dot{V}_{O_2}$, respectively, P<0.05).

Muscle citrate synthase activity

The mass-specific CS activity was evaluated according to the allometric scaling relationship, as described above. CS activity was independent of body mass, with a b value of 0.09 that was not significantly different from zero (Fig. 4).

Muscle arginine phosphate recovery rate

The tail-flipping stimulation procedure elicited a burst escape response in the three species and size classes, although the number of tail-flips to exhaustion was species specific (see below). Fig. 5 shows the changes in AP concentration during the initial phase of recovery. As expected, muscles from smaller species recovered with a significantly higher rate than in larger species (ANCOVA: F=32.86, P<0.0001). However, within each species, there were no significant differences in recovery rate between the small and large size classes (ANCOVA: *P. pugio*, F=0.33, P=0.57; *Penaeus* spp., F=0.27, P=0.61; *P. argus*, F=0.05, P=0.82). Fig. 6 shows the scaling relationships with body mass of AP recovery, whole-animal post-exercise O_2 consumption, and muscle CS activity, using means for all data to correspond with the AP recovery data. The body-mass scaling exponent for AP recovery (b=–0.12) was less than whole-animal post-tail flip O_2 consumption (b=–0.21), but greater

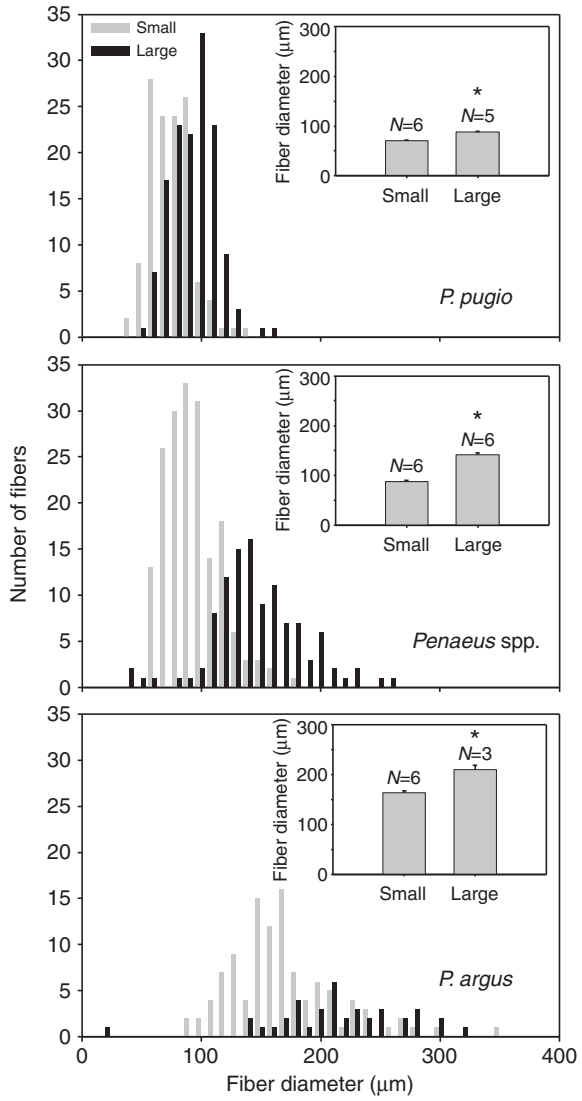

Fig. 3. Abdominal white muscle fiber diameter distribution and mean diameter (inset) from each size class of the three species of crustaceans, *P. pugio*, *Penaeus spp.* and *P. argus*. Fiber size was significantly different between size classes within each species (Student's *t*-test, $P<0.05$). Values are means ± s.e.m.

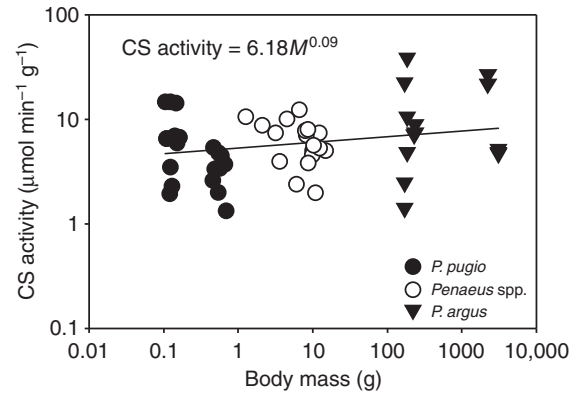

Fig. 4. Scaling with body mass of citrate synthase (CS) activity from abdominal white muscle of each size class and species of crustacean. The scaling exponent, *b*, was 0.09 (r^2=0.11, $P<0.05$).

than muscle oxidative capacity, indexed by CS activity (b=0.09) (Fig. 6).

Muscle L-lactate concentration

The lactate concentration was determined immediately after exercise and after 15 min of recovery. The lactate concentration immediately after contraction was not significantly different from the concentration 15 min after contraction for either size class in any of the three species (Fig. 7). However, limited animal availability for lactate assays in the large *P. argus* size class prevented statistical analysis within this group. Nevertheless, post-contractile anaerobic metabolism does not appear to be an important component of recovery in these species, despite a wide variation in animal body mass and fiber sizes. The contractile production of lactate varied between species mostly owing to the varying number of tail-flips

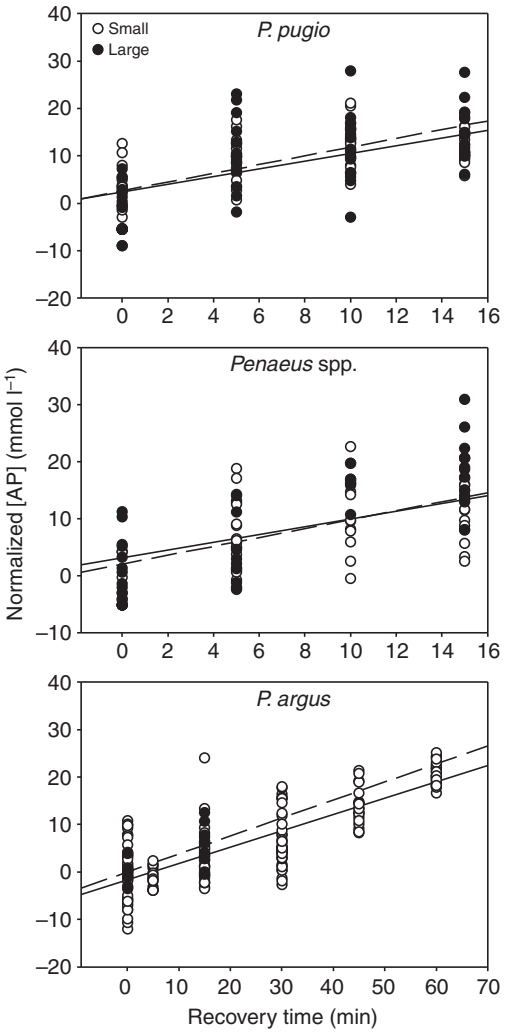

Fig. 5. The initial rate of post-tail flip arginine phosphate (AP) recovery for the small (broken lines) and large (unbroken lines) size classes. Linear regressions for small and large *P. pugio* resulted in r^2 values of 0.36 and 0.43 and regression equations of y=0.92x+2.61 and y=0.81x+2.40, respectively. Small and large *Penaeus* spp. had r^2 values of 0.60 and 0.23 and regression equations of y=0.78x+1.97 and y=0.68x+3.08, respectively. Small and large *P. argus* yielded r^2 values of 0.68 and 0.42 and regression equations of y=0.34x–1.72 and y=0.38x+0, respectively. All regression slopes were significantly different from zero ($P<0.05$), but recovery rates between the small and large size classes were not significantly different within any species (see text).

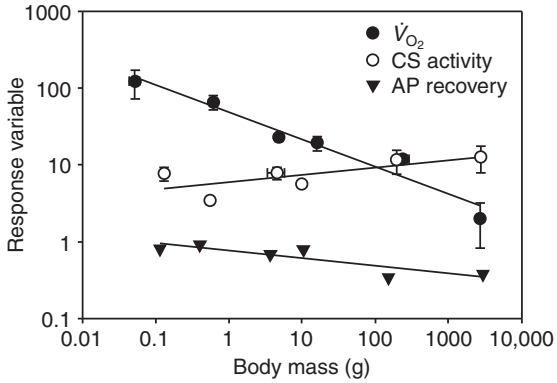

Fig. 6. Comparison of the relationship between the scaling with body mass of whole-animal metabolic rate ($\dot{V}_{O_2}$), muscle aerobic capacity (CS activity) and a muscle metabolic process (AP resynthesis) following tail-flipping responses in three species of crustaceans. Data are reported as means ± s.e.m. All regression slopes were significantly different from zero except for CS activity ($\dot{V}_{O_2}$=32.0M$^{-0.21}$, r^2=0.95, P<0.05; AP resynthesis rate=1.22M^{-012}, r^2=0.77, P<0.05; CS activity=6.18M$^{0.09}$, r^2=0.68).

performed during the exercise protocol (Fig. 7). This variation occurred despite the fact that all species tail-flipped a number of times that was equal to half the number that induced exhaustion (see Materials and methods).

Mathematical modeling

Fig. 8 shows model calculations of the ATP turnover rate as a function of the rate constants governing ATP demand (k_1) and ATP supply (k_2) for the case without diffusion (Eqn 8, which defines the denominator in the calculation of η) for a given cell size and O_2 concentration at the boundary. This figure shows that, for a constant value of k_1, the reaction rate from the model increases with increasing k_2 until it asymptotically approaches a limiting value at very large k_2. Thus, it is clear that the ATP demand (k_1) sets an upper limit on the rate of ATP turnover. In addition, these results show that more than one combination of k_1 and k_2 can be used to give the experimentally observed rate of ATP turnover. The smallest value of k_1 at asymptotically large k_2 that matches the experimentally observed ATP turnover rate was determined for each condition of O_2 concentration at the boundary and cell size, and it was found (data not shown) that the highest average ATP and O_2 concentrations occurred at this value of k_1.

Fig. 9A shows the dependence of the ATP turnover rate on the values of k_1 and k_2 for the case with diffusion (Eqn 9, which defines the numerator in the calculation of η). As with the no-diffusion case, many combinations of k_1 and k_2 can yield the experimentally observed ATP turnover rate. The minimum value of k_1 that would allow the model to satisfy the observed ATP turnover rate was determined by trial and error, and these values were slightly larger than the minimum k_1 values determined for the no-diffusion cases mentioned above. The corresponding k_2 values for these minimum values of k_1 were determined using a root-finding method. As in the cases without diffusion, it was found in the cases with diffusion that the lowest possible values of k_1 lead to the highest average ATP and O_2 concentrations. These cases also lead to the largest effectiveness factors, and Fig. 9B shows the corresponding relationship of k_1 and k_2 to the effectiveness factor.

Our model calculations represent a conservative approach to the analysis of diffusion limitation, whereby kinetic parameters were identified that led to the highest possible values of η, and therefore the lowest possible extent of diffusion limitation. The values of the rate constants are not known in the present model; however, these values reflect the capacities for mitochondrial and ATPase reactions and are grounded in experimentally measured rates of AP recovery.

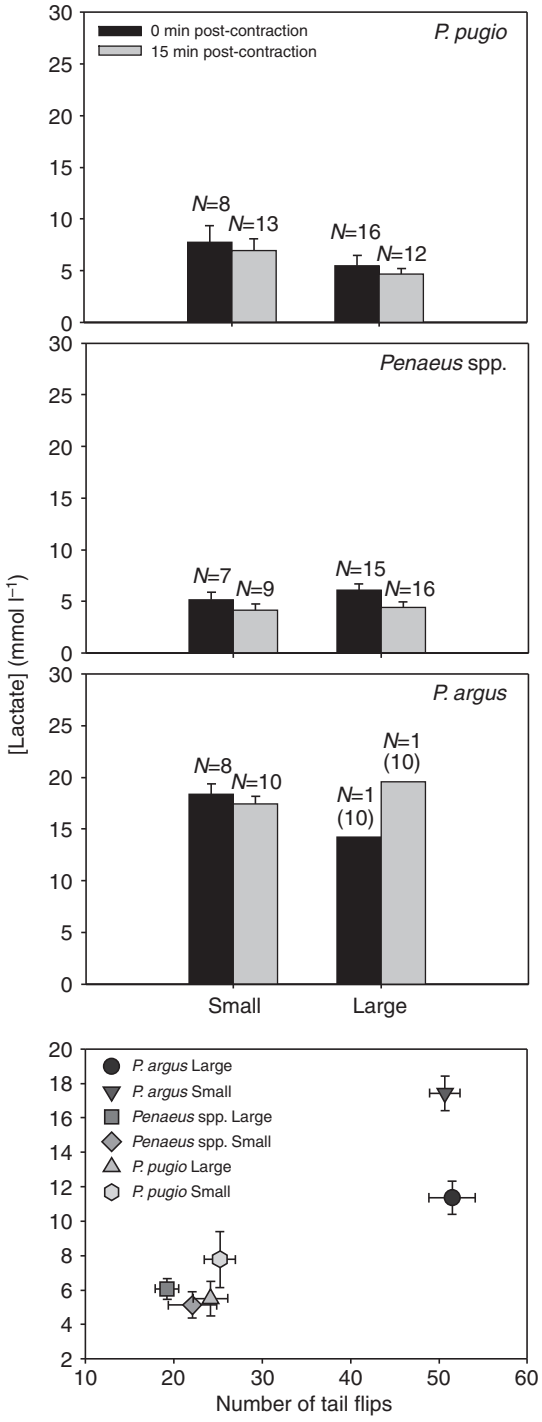

Fig. 7. Lactate levels immediately after exercise (black bars) and after 15 min of recovery (gray bars), as well as the relationship between contractile lactate production and number of tail flips. Lactate accumulation did not increase significantly after 15 min of recovery in any group. However, as only two specimens of the large *P. argus* were available for lactate measurement (one for each time point), a statistical analysis was not possible for this group (numbers in parentheses for large *P. argus* represent replicates within a single specimen). Values are means ± s.e.m.

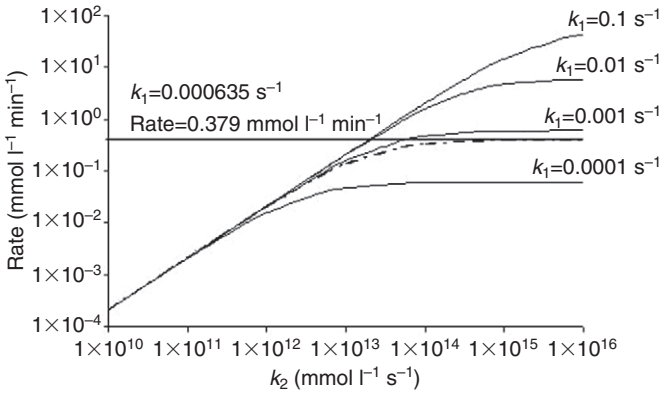

Fig. 8. Mathematical model of reaction rate for the case without diffusion as a function of the two reaction rate constants with a fixed diffusion distance (L=104.5 μm) and O_2 boundary concentration of 7.85 μM. The broken line is for the case of k_1=0.000635 s^{-1}, which satisfies the experimentally measured rate of AP recovery of 0.379 mmol l^{-1} min^{-1} in the limit of large k_2.

Using this approach, intracellular concentration gradients are apparent in O_2, but not ATP, as is illustrated for the three O_2 concentrations for the smallest and largest fiber sizes in Fig. 10. It is implicit in the model utilized here that the ATP will have no or minimal concentration gradient because of the two no-flux boundary conditions for ATP and ADP. Despite the presence of oxygen concentration gradients, which have typically been used as a proxy for diffusion limitation, the influence of these gradients on ATP turnover is small at the high and intermediate O_2 concentrations, as indicated by the relatively high effectiveness factors for all fiber sizes and experimentally observed AP recovery rates (Table 1). This means that the measured rate of AP recovery is *too slow* to be substantially limited by diffusion of oxygen or HEP metabolites. By contrast, effectiveness factors were consistently lower at the lowest O_2 concentration (Table 1). It should be noted that, for each species, diffusion limitation increased as the fibers grow larger. These developmental trajectories are presented graphically in Fig. 11, but, in this case, a single value of k_1 was used in order to capture the behavior of η for all species and size classes. Clearly, all species become more diffusion limited as they grow, and it is also noteworthy that here the effectiveness factors are much lower when k_1 and k_2 are not selected to maximize η, indicating substantial diffusion limitation in the adult animals.

DISCUSSION

The major finding of the present study was that whole-animal post-exercise $\dot{V}_{O_2}$ had a more negative body-mass scaling exponent (b) than post-contractile muscle AP recovery, and AP recovery, in turn, had a more negative scaling exponent than muscle CS activity. Post-contractile lactate accumulation was not significant, and anaerobic metabolism therefore does not appear to play a major role in the recovery rate of AP in the three groups examined. A mathematical reaction–diffusion model yielded relatively high effectiveness factors for all species except at the lowest hemolymph P_{O_2}, indicating that the observed rates of muscle AP recovery might not be substantially limited by diffusion under most conditions. However, the decrease in effectiveness factors associated with increased fiber size suggests that at least some of the difference in the scaling of muscle aerobic capacity (indicated by CS activity) and an aerobic process (AP resynthesis) might be due to diffusion limitation.

In all species, fibers grew hypertrophically, and fiber size within and across species was proportional to body mass. Hypertrophic growth leads to developmental increases in diffusion distances that limit the permissible rates of intracellular aerobic processes (Kinsey et al., 2007). Changes in fiber dimensions occur despite the fact that the burst escape-and-recovery function of the muscles remained essentially the same in juvenile and adult animals. Owing to the greater diffusion distances, we expected to find increased diffusion limitation of aerobic processes in larger fibers. For instance, the time, t, required for a particle to traverse a given distance by diffusion is described by $t=\lambda^2/2D$, where λ is the root-mean-square displacement and D is the diffusion coefficient. Therefore, the time required for O_2 or ATP to diffuse from the sarcolemma to the center of a fiber from the large size class of *P. argus* is approximately nine times longer than in a fiber from the small size class of *P. pugio*. Previous work on hypertrophically growing crustaceans and fish anaerobic fibers has shown that diffusion limitation of AP recovery

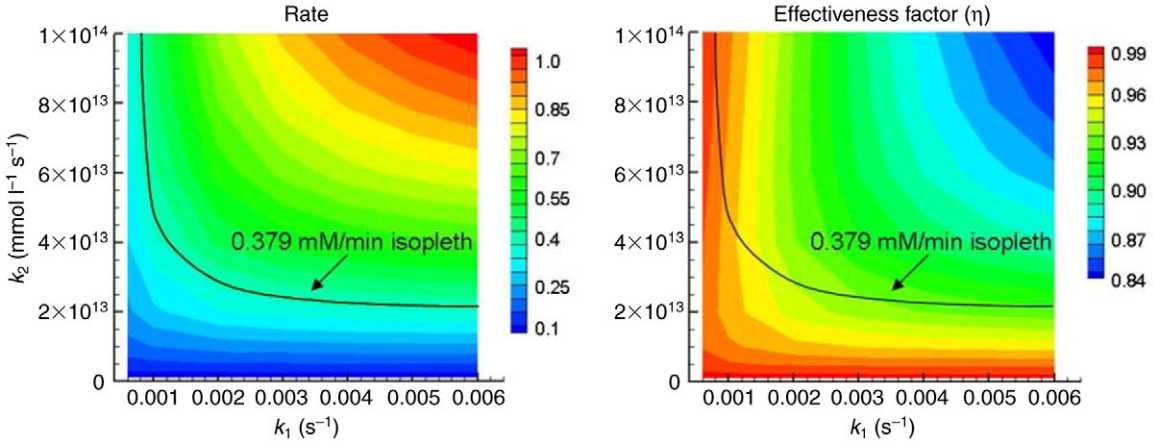

Fig. 9. Example of mathematical modeling of reaction rate and effectiveness factor for the case with diffusion for various values of k_1 and k_2 with a fixed diffusion distance (L=104.5) and O_2 boundary concentration of 7.85 μmol l^{-1}. The experimentally measured rate of AP recovery of 0.379 mmol l^{-1} min^{-1} is indicated by the unbroken line, which shows the range of values of k_1 and k_2 that satisfy this rate (left panel), and the corresponding effectiveness factor (right panel). Values of k_1 and k_2 that satisfied the observed rate and maximized the effectiveness factor were then determined using a root-finding method (see text).

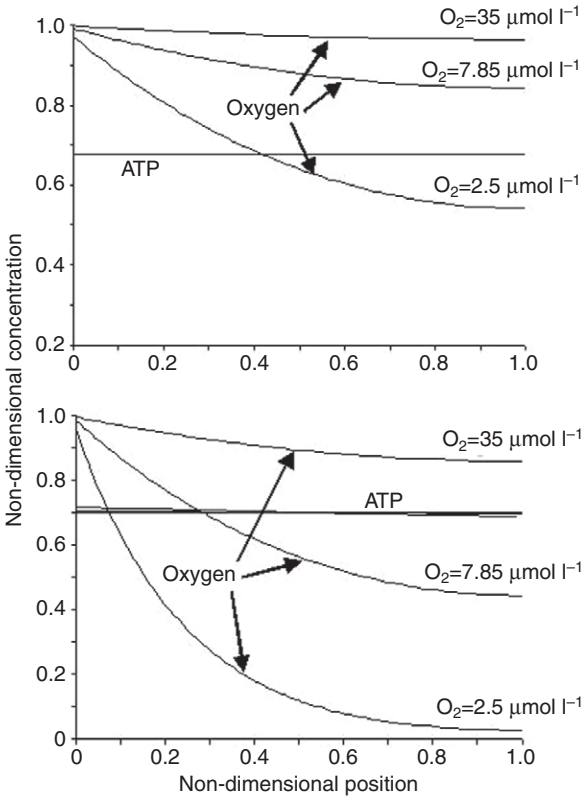

Fig. 10. Examples of reaction–diffusion model output for the smallest and largest fibers. (Top panel) O_2 and ATP concentration profiles for muscle from small *P. pugio*, where the diffusion distance is 35.1 μm and the AP recovery rate is 0.811 mmol l^{-1} min^{-1}. (Bottom panel) O_2 and ATP concentration profiles for muscle from large *P. argus*, where the diffusion distance is 104.5 μm and the AP recovery rate is 0.379 mmol l^{-1} min^{-1}. Other data from the model for all species and size classes are in Table 1.

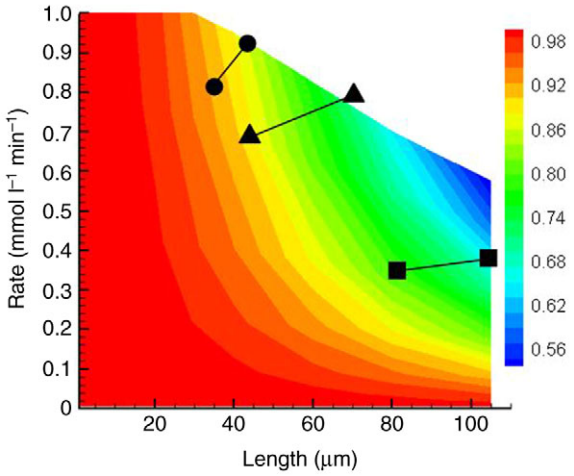

Fig. 11. Effectiveness factor as functions of rate and diffusion distance compared with the experimental data. The ATPase rate constant k_1 is fixed for all species and size classes, where k_1=0.008 s^{-1}. Here, k_2 was varied to generate the various rates, and the intermediate O_2 concentration of 7.85 μmol l^{-1} was used for both cases. The unbroken lines connect the juvenile and adults of each species, where the circles are *P. pugio*, the triangles are *Penaeus* spp., and the squares are *P. argus*. Note that η decreases for each species as the animals grow.

is indeed highest in adult animals (Boyle et al., 2003; Kinsey et al., 2005; Nyack et al., 2007). These prior studies examined only HEP diffusion, and the authors suggested that low SA:V and associated limitations on the diffusion of O_2 across the sarcolemma might be more important than HEP diffusion in constraining the rate of aerobic recovery after burst-contractions (see below).

The standard metabolic rates measured in our current study were consistent with previous studies of species of *Panulirus* (Winget, 1969; Buesa, 1979; Diaz-Iglesias et al., 2004), *Penaeus* (Bishop et al., 1980; Dall, 1986; Villareal and Ocampo, 1993) and *Palaeomonetes* (MacFarland and Pickens, 1965) (Fig. 2). The observed increase in O_2 consumption after several bouts of exercise was expected. In both size classes of *P. argus* and *Penaeus* spp., the exercise regimen caused an approximately 2.3-fold increase in $\dot{V}_{O_2}$, whereas there was a 3.2-fold increase in $\dot{V}_{O_2}$ for the much smaller *P. pugio*. This is consistent with prior studies that have shown that increases in activity commonly cause a three- to five-fold increase in O_2 uptake in aquatic crustaceans (Taylor, 1982; Full and Herreid, 1983; Hamilton and Houlihan, 1992; McGraw, 2007), although a 10-fold increase in O_2 uptake after exercise has been found in the tail-flipping crayfish *Pacifastacus leniusculus* (Taylor, 1982). It should be noted, however, that the relatively small fold-increase in metabolic rate in the present study results in part from the fact that the increases in post-exercise $\dot{V}_{O_2}$ were relative to standard $\dot{V}_{O_2}$, whereas some of the other cited studies compared the increase with basal $\dot{V}_{O_2}$. The scaling with body mass of post-exercise $\dot{V}_{O_2}$ (b=–0.21) and standard $\dot{V}_{O_2}$ (b=–0.18) was similar to that previously observed in crustaceans (MacFarland and Pickens, 1965; Bridges and Brand, 1980; Zoutendyk, 1989; Martinez Palacios et al., 1996) (Fig. 2).

The rates of AP recovery were also similar to values previously reported for anaerobic muscle from fishes (Curtin et al., 1997; Hardewig et al., 1998; Nyack et al., 2007), mollusks (Bailey et al., 2003) and other crustaceans (Onnen and Zebe, 1983; Hansen et al., 1986; Morris and Adamczewska, 2002; Boyle et al., 2003). Data from the three species used in the present study had a combined body mass scaling exponent of –0.12 (Fig. 6), which is similar to the overall scaling exponent of –0.14 obtained when data from the present study were combined with published results for white muscle of similar aerobic capacity (Fig. 12). Likewise, the positive scaling with body mass of CS activity (b=0.09) is consistent with prior studies of anaerobic muscle. CS is a key regulatory enzyme in the citric acid cycle and gives a quantitative estimate of aerobic capacity (Berges and Ballantyne, 1991), although it should be noted that measures of activity might not necessarily reflect rates of *in vivo* flux through the reaction. CS activity in skeletal muscle often has an inverse relationship with body mass, but the slope is usually less steep than the slope for mass-specific standard metabolic rate (Childress and Somero, 1990; Somero and Childress, 1990; Emmett and Hochachka, 1981). Other studies have found white muscle CS activity to scale positively with body mass, as in the present study (Berges and Ballantyne, 1991), or to have a slope near zero (Wells et al., 2001; Boyle et al., 2003; Nyack et al., 2007).

If diffusion is limiting metabolism in muscle, we would expect the scaling exponent for AP recovery to be more negative than that for $\dot{V}_{O_2}$ or CS activity as fiber size (and therefore diffusion distance) was proportional to body mass. Using this criterion, diffusion might account for the difference in scaling of AP recovery rate and CS activity, but not AP recovery rate and $\dot{V}_{O_2}$, as $\dot{V}_{O_2}$ had the most negative scaling exponent. In addition, if diffusion were limiting, we would expect to find evidence that the rate of an observed aerobic process (i.e. AP recovery) is, in fact, less than it would be if it were

Table 1. Summary of maximum effectiveness factors (η), average non-dimensional O_2 ($<C_{O_2}>$) and ATP concentrations ($<C_{ATP}>$), and k_1 and k_2 values for three blood O_2 concentration (C^o) cases and experimentally determined diffusion path lengths and AP recovery rates

Species and size	C^o (μmol l^{-1})	Length (μm)	AP recovery rate (mmol l^{-1} min^{-1})	$<C_{O_2}>$ (μmol l^{-1})	$<C_{ATP}>$ (mmol l^{-1})	k_1 (s^{-1})	k_2 (1/mmol l^{-1} s^{-1})	η
P. pugio small	2.50	32.1	0.811	0.67	0.67	0.0020	2.46×10^{15}	0.90
P. pugio large	2.50	43.8	0.922	0.49	0.61	0.0025	3.24×10^{15}	0.81
Penaeus spp. small	2.50	44.1	0.684	0.59	0.56	0.0020	1.70×10^{15}	0.84
Penaeus spp. large	2.50	70.7	0.789	0.23	0.52	0.0025	4.80×10^{15}	0.65
P. argus small	2.50	81.8	0.344	0.41	0.63	0.0009	1.52×10^{15}	0.79
P. argus large	2.50	104.5	0.379	0.23	0.70	0.0009	3.83×10^{15}	0.77
P. pugio small	7.85	32.1	0.811	0.88	0.45	0.0016	1.25×10^{15}	0.86
P. pugio large	7.85	43.8	0.922	0.81	0.51	0.0018	1.64×10^{15}	0.91
Penaeus spp. small	7.85	44.1	0.684	0.85	0.56	0.0014	9.08×10^{14}	0.80
Penaeus spp. large	7.85	70.7	0.789	0.62	0.43	0.0019	8.69×10^{14}	0.94
P. argus small	7.85	81.8	0.344	0.77	0.57	0.0007	5.27×10^{14}	0.92
P. argus large	7.85	104.5	0.379	0.61	0.62	0.0008	6.25×10^{15}	0.95
P. pugio small	35.33	32.1	0.811	0.97	0.67	0.0015	4.00×10^{14}	0.99
P. pugio large	35.33	43.8	0.922	0.95	0.76	0.0020	1.95×10^{14}	0.99
Penaeus spp. small	35.33	44.1	0.684	0.96	0.56	0.0020	7.80×10^{13}	0.99
Penaeus spp. large	35.33	70.7	0.789	0.90	0.65	0.0015	3.30×10^{14}	0.97
P. argus small	35.33	81.8	0.344	0.94	0.57	0.0007	9.50×10^{13}	0.98
P. argus large	35.33	104.5	0.379	0.90	0.63	0.0009	6.60×10^{13}	0.97

Values were obtained at the lowest values of k_1 that satisfied the observed rate.

dependent on catalytic capacity alone. To address this issue, we developed a reaction–diffusion mathematical model to assess the extent to which diffusion might limit AP recovery in muscle and therefore possibly influence scaling behavior. The effectiveness factor (η) was employed here because it represents a means of evaluating the influence of diffusion on metabolic flux. We used a very conservative approach, where the kinetic properties that dictate ATP turnover, k_1 and k_2, were generated in a way that would yield the highest possible effectiveness factor. This resulted in high η values for the high and intermediate O_2 concentrations, whereas effectiveness factors were lower at the lowest O_2 concentration. This suggests that, when animals are faced with environmental hypoxia or undergo intense exercise, a potential decrease in blood P_{O_2} might cause a greater diffusion limitation that possibly constrains the rate of metabolic recovery (Table 1; Fig. 11). This is consistent with the observation that reduced arterial P_{O_2} during hypoxia can inhibit aerobic metabolic processes in crustacean muscle (Mende et al., 2003) despite a variety of compensatory responses designed to preserve O_2 delivery, such as an increased rate of ventilation and blood shunting to the muscle (McMahon, 2001). In fact, the scaling exponent of η at the lowest P_{O_2} (b=–0.10) was equal to one half of the difference in b values between CS activity and AP recovery rate, lending some support to the notion that diffusion is partly responsible for the difference.

It is also clear from Fig. 10 that concentration gradients for O_2 are substantial in all cases, and gradients increase with either increasing fiber size or decreasing blood P_{O_2}. This is consistent with prior suggestions that O_2 delivery is a greater constraint on muscle design and function than is HEP diffusion (Kinsey et al., 2005; Hardy et al., 2006; Nyack et al., 2007). This is in agreement with the notion that the shift in mitochondrial distribution towards the periphery of fibers that occurs during muscle growth in some crustacean and fish white muscle is a response to strong O_2 gradients in the large fibers of adult animals (Boyle et al., 2003; Nyack et al., 2007). As we do not have data on mitochondrial distribution for the species used in the present study, we assumed a uniform distribution, which is consistent with previous measurements in blue crab muscle fibers of a size comparable to those analyzed here (Boyle et al., 2003). However, Mainwood and Rakusan (Mainwood and Rakusan, 1982) showed mathematically that a peripheral mitochondrial distribution reduced the intracellular concentration gradient for O_2 and led to better spatial buffering of ATP concentration across the fiber. Thus, a non-uniform organization of mitochondria might reduce diffusion effects. We also did not include in our analysis the possibility that arginine kinase is localized to different regions within the cell, and that this might reduce the magnitude of concentration gradients in HEP compounds. While data for arginine kinase localization in

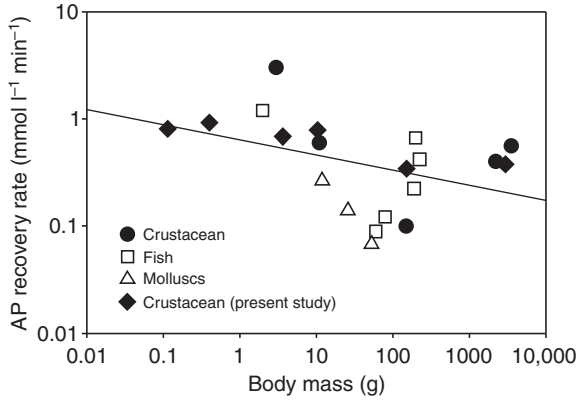

Fig. 12. Scaling with body mass of the AP/PCr recovery rate in white muscle from crustaceans (*Crangon crangon*, *Gecarcoidea natalis*, *Callinectes sapidus*), fishes (*Oncorhynchus mykiss*, *Salmo gairdnei*, *Pachycara brachycephalum*, *Zoarces viviparus*, *Squalus acanthias*, and three size classes of *Centropristis striata*), mollusks (*Placopecten magellanicus*, *Aequipecten percularis*, *Adamussium colbecki*) and the crustaceans from our current study. The regression line is described by the equation, recovery rate=1.56M$^{-0.14}$ (r^2=0.16, P<0.05). The recovery rates and body mass data for other species were obtained from the published literature (Onnen and Zebe, 1983; Hansen et al., 1986; Curtin et al., 1997; Hardewig et al., 1998; Morris et al., 2002; Bailey et al., 2003; Johnson et al., 2004; Nyack et al., 2007; Livingstone et al. 1981; Wang et al., 1994; Richards et al., 2003).

Table 2. Percentage of $\dot{V}_{O_2}$ devoted to AP resynthesis in the abdominal muscle

Species and size	ATP demand from $\dot{V}_{O_2}$ data (μmol ATP g^{-1} min^{-1})	ATP demand from AP recovery (μmol ATP g^{-1} min^{-1})	Abdominal muscle (% of body mass)	Percentage of $\dot{V}_{O_2}$ going to AP resynthesis
P. pugio small	32.44	0.5677	64	1.12
P. pugio large	17.56	0.6454	52	1.93
Penaeus spp. small	6.08	0.4788	60	4.73
Penaeus spp. large	5.181	0.5523	59	6.30
P. argus small	3.184	0.2408	35	2.65
P. argus large	0.534	0.2653	36	17.70

Whole-animal $\dot{V}_{O_2}$ and AP recovery rates were directly compared by measurement of the percentage of body mass that is abdominal muscle, and assuming 22.4 litre O_2 mol^{-1} O_2, an ATP/O_2 ratio of 6 and an intracellular water content that was 70% of wet mass.

crustacean anaerobic fibers are limited, the role of phosphagen kinase localization on diffusion-dependent processes is typically considered to be important only in highly aerobic fibers (reviewed in Ellington, 2001). Furthermore, we found very slight gradients for HEP compounds when we assumed a homogeneous arginine kinase reaction, so the potential impact of increasing the model complexity to account for localization is negligible.

While some of the considerations described above imply that diffusion effects might be less than we reported, it is also plausible that diffusion limitation in muscle is more extreme than indicated in our analysis. For instance, the AP recovery rate might substantially underestimate total ATP turnover during recovery, which could lead to a dramatically increased effectiveness factor. Tail-flipping caused large metabolic perturbations leading to a 2.3- to 3.2-fold increase in whole-animal $\dot{V}_{O_2}$ above standard $\dot{V}_{O_2}$ due to activating the abdominal muscle group. However, we estimated the relative cost of AP recovery and found that the percentage of post-exercise $\dot{V}_{O_2}$ devoted to AP recovery was body size dependent and ranged from only 1% in small *P. pugio* to 17% in large *P. argus* (Table 2). In other words, only a small fraction of metabolic recovery following tail flipping is devoted to AP recovery, which suggests that other processes in the muscle, such as pH and ionic gradient restoration, lactate processing and glycogen resynthesis might be additional important sources of ATP demand (Full and Herreid, 1983).

A possible explanation for the observed differences in whole-animal $\dot{V}_{O_2}$ and AP recovery is that anaerobic metabolism might contribute more to AP recovery in large fibers than in small fibres, thus leading to a less-negative scaling exponent. We hypothesized that anaerobic metabolism would be used to speed up the recovery process in large animals to compensate for diffusion constraints associated with large fiber size. In the blue crab, for example, anaerobic metabolism is used to speed up AP recovery following exercise, as shown by the observation that large muscle fibers continue to accumulate large amounts of lactate after contraction, whereas lactate accumulation is minimal in small fibers (Johnson et al., 2004). This led to a higher than expected rate of AP recovery in the fibers of the largest blue crabs (Kinsey et al., 2005). However, there was no evidence of post-contractile lactate accumulation in the present study, suggesting that anaerobic metabolism is not invoked to accelerate recovery. The greater lactate production observed during contraction (at time zero after contraction; Fig. 7) is consistent with previous work on tail-flipping yabbies, which demonstrated positive allometry for contractile lactate production as well as anaerobic capacity (Baldwin et al., 1999).

In summary, we found different scaling exponents for whole-animal $\dot{V}_{O_2}$, muscle CS activity and muscle AP recovery in three groups of tail-flipping crustaceans. Muscle fibers grew hypertrophically and varied in mean diameter from 70 to 210 μm, leading to substantially greater intracellular diffusion distances in larger animals. A mathematical model revealed that fibers became more diffusion limited as they got larger, particularly when hemolymph P_{O_2} was low. Diffusion might, therefore, account for some of the differences in scaling exponents, although in most cases diffusion limitation was minimal. The large differences in scaling exponents probably also reflect different mechanisms of control affecting each measured variable, which is consistent with the notion that scaling exponents of complex processes represent aggregate functions that reflect the scaling behavior of the underlying components (Darveau et al., 2002).

We thank Dr Barry Ache and Dr Juan Aggio for donating small *P. argus*; Captain Gerry Compeau, Dave Wells, Jay Souza, Steve Hall and Jennifer Dorton for collecting large *P. argus*; Clark Gray and Rodney Hayward for collecting penaeid shrimp; Dr M. Bailey from the University of Aberdeen, UK, for some of the data provided in Fig. 12; Dr Chris Finelli for helping with graphs and figures; and Mark Gay and Dr Dick Dillaman for their assistance with microscopy. This study was funded by National Science Foundation grants to S.T.K. (IOS-0316909 and IOS-0719123) and B.R.L. (IOS-0315883 and IOS-0718499), a National Institutes of Health grant to S.T.K. (NIAMS R15-AR052708) and a Sigma-Xi grant to A.G.J.

REFERENCES

Bailey, D. M., Peck, L. S., Bock, C. and Pörtner, H. O. (2003). High-energy phosphate metabolism during exercise and recovery in temperate and Antartic scallops: an in vivo ^{31}P-NMR study. *Physiol. Biochem. Zool.* **76**, 622-633.

Baldwin, J., Gupta, A. and Iglesias, X. (1999). Scaling of anaerobic energy metabolism during tail flipping behaviour in the freshwater crayfish, *Cherax destructor*. *Mar. Freshw. Res.* **50**, 183-187.

Berges, J. A. and Ballantyne, J. S. (1991). Size scaling of whole-body maximal enzyme activities in aquatic crustaceans. *Can. J. Fish. Aquat. Sci.* **48**, 2385-2394.

Bishop, J. M., Gosselink, J. G. and Stone, J. H. (1980). Oxygen consumption and hemolymph osmolality of brown shrimp, *Penaeus aztecus*. *Fish Bull. (Wash. DC)* **78**, 741-757.

Bittner, G. D. and Traut, D. L. (1978). Growth of crustacean muscles and muscle fibers. *J. Comp. Physiol.* **124**, 277-285.

Booth, C. E. and McMahon, B. R. (1985). Lactate dynamics during locomotor activity in the blue crab, *Callinectes sapidus*. *J. Exp. Biol.* **118**, 461-465.

Boyle, K. M., Dillaman, R. M. and Kinsey, S. T. (2003). Mitochondrial distribution and glycogen dynamics suggest diffusion constraints in muscle fibers of the blue crab, *Callinectes sapidus*. *J. Exp. Zool.* **297A**, 1-16.

Bridges, C. R. and Brand, A. R. (1980). Oxygen consumption and oxygen-independence in marine crustaceans. *Mar. Ecol. Prog. Ser.* **2**, 133-141.

Buesa, R. J. (1979). Oxygen consumption of the two tropical spiny lobsters *Panulirus argus* (Latreille) and *P. guttatus* (Latreille) (Decapoda, Palinuridae). *Crustaceana* **36**, 99-107.

Childress, J. J. and Somero, G. N. (1990). Metabolic scaling: a new perspective based on scaling of glycolytic enzyme activities. *Am. Zool.* **30**, 161-173.

Curtin, N. A., Kushmerick, M. J., Wiseman, R. W. and Woledge, R. C. (1997). Recovery after contraction of white muscle fibers from the dogfish, *Scyliorhimus canicula*. *J. Exp. Biol.* **200**, 1061-1071.

Dall, W. (1986). Estimation of routine metabolic rate in penaid prawn, *Penaeus esculentus* Haswell. *J. Exp. Mar. Biol. Ecol.* **96**, 57-74.

Darveau, C.-A., Suarez, R. K., Andrews, R. D. and Hochachka, P. W. (2002). Allometric cascade as unifying principle of body mass effects on metabolism. *Nature* **417**, 166-170.

Díaz-Iglesias, E., Díaz-Herrera, F., Re-Araujo, A. D., Báez-Hidalgo, M., López-Zenteno, M., Valdés-Saáchez, G. and López-Murillo, A. K. (2004). Temperature preference and circadian oxygen consumption of the red spiny lobster, *Panulirus interruptus* (Randall, 1842). *Cienc. Mar.* **30**, 169-178.

Ellington, W. R. (2001). Evolution and physiological roles of phosphagen systems. *Ann. Rev. Physiol.* **63**, 289-325.

Emmett, B. and Hochachka, P. W. (1981). Scaling of oxidative and glycolytic enzymes in mammals. *Respir. Physiol.* **45**, 261-272.

England, W. R. and Baldwin, J. (1983). Anaerobic energy metabolism in the tail musculature of the Australian yabby *Cherax destructor*: role of phosphagens and anaerobic glycolysis during escape behavior. *Physiol. Zool.* **56**, 614-622.
Forgue, J., Legeay, A. and Massabuau, J.-C. (2001). Is the resting rate of oxygen consumption of locomotor muscle in crustaceans limited by the low blood oxygenation strategy? *J. Exp. Biol.* **204**, 933-940.
Full, R. J. and Herreid, C. F. (1983). Aerobic response to exercise of the fastest land crab. *Am. J. Physiol.* **244**, R530-R536.
Hamilton, N. M. and Houlihan, F. R. (1992). Respiratory and circulatory adjustments during aquatic treadmill exercise in the European shore crab *Carcinus maenas*. *J. Exp. Biol.* **162**, 37-54.
Hansen, J., Sharpe, T. and Bittar, E. E. (1986). Phosphate metabolites in single barnacle muscle fibers investigated by phosphorus-31 nuclear magnetic resonance. *Comp. Biochem. Physiol.* **83B**, 875-879.
Hardewig, I., Van Dijk, P. L. M. and Pörtner, H. O. (1998). High-energy turnover at low temperatures: recovery from exhaustive exercise in Antarctic and temperate eelpouts. *Am. J. Physiol. Regul. Integr. Comp. Physiol.* **274**, 1789-1796.
Hardy, K. M., Locke, B. R., Da Silva, M. and Kinsey, S. T. (2006). A reaction-diffusion analysis of energetics in large muscle fibers secondarily evolved for aerobic locomotion. *J. Exp. Biol.* **209**, 3610-3620.
Head, G. and Baldwin, J. (1986). Energy metabolism and the fate of lactate during recovery from exercise in the Australian freshwater crayfish *Cherax destructor*. *Aust. J. Mar. Freshw. Res.* **37**, 641-646.
Henry, R. P., Booth, C. E., Lallier, F. H. and Walsh, P. J. (1994). Post-exercise lactate production and metabolism in three species of aquatic and terrestrial decapod crustaceans. *J. Exp. Biol.* **186**, 215-234.
Hoyle, G., McNeill, P. A. and Selverston, A. I. (1973). Ultrastructure of barnacle giant muscle fibers. *J. Cell Biol.* **56**, 74-91. .
Hubley, M. J., Locke, B. R. and Moerland, T. S. (1997). Reaction-diffusion analysis of the effects of temperature on high energy phosphate dynamics in goldfish skeletal muscle. *J. Exp. Biol.* **200**, 975-988.
Johnson, L. K., Dillaman, R. M., Gay, D. M., Blum, J. E. and Kinsey, S. T. (2004). Metabolic influences of fiber size in aerobic and anaerobic locomotor muscles of the blue crab, *Callinectes sapidus*. *J. Exp. Biol.* **207**, 4045-4056.
Kinsey, S. T. and Ellington, W. R. (1996). ^{1}H- and ^{31}P-Nuclear magnetic resonance studies of L-lactate transport in isolated muscle fibers from the spiny lobster, *Panulirus argus*. *J. Exp. Biol.* **199**, 2225-2234.
Kinsey, S. T. and Moerland, T. S. (2002). Metabolite diffusion in giant muscle fibers of the spiny lobster *Panulirus argus*. *J. Exp. Biol.* **205**, 3377-3386.
Kinsey, S. T., Pathi, P., Hardy, K. M., Jordan, A. and Locke, B. R. (2005). Does intracellular metabolite diffusion limit post-contractile recovery in burst locomotor muscle? *J. Exp. Biol.* **208**, 2641-2652.
Kinsey, S. T., Hardy, K. M. and Locke, B. R. (2007). The long and winding road: influences of intracellular metabolite diffusion on cellular organization and metabolism in skeletal muscle. *J. Exp. Biol.* **210**, 3505-3512.
Livingstone, D. R., De Zwaan, A. and Thompson, R. J. (1981). Aerobic Metabolism, octopine production and phosphoarginine as sources of energy in the phasic and catch adductor muscles of the giant scallop *Placopecten magellanicus* during swimming and subsequent recovery period. *Comp. Biochem. Physiol.* **70B**, 35-44.
Locke, B. and Kinsey, S. T. (2008). Diffusional constraints on energy metabolism in skeletal muscle. *J. Theor. Biol.* **254**, 417-429.
Lowry, O. H. and Passonneau, J. V. (1972). Lactate: method II. In *A Flexible System of Enzymatic Analysis*. New York: Academic Press.
Kushmerick, M. (1983). Energetics of muscle contraction. In *Handbook of Muscle Physiology-Skeletal Muscle* (ed. L. D. Peachy, R. H. Adrian and S. R. Geiger), pp. 189-236. Bethesda, MD: American Physiological Society.
MacFarland, W. N. and Pickens, P. E. (1965). The effects of season, temperature, and salinity on standard and active oxygen consumption of the grass shrimp *Palaemonetes vulgaris* (Say). *Can. J. Zool.* **43**, 571-585.
Mainwood, G. W. and Rakusan, K. (1982). A model for intracellular energy transport. *Can. J. Physiol. Pharmac.* **68**, 98-102.
Martinez Palacios, C. A., Ross, L. G. and Jimenez Valenzuela, L. (1996). The effects of temperature and body weight on the oxygen consumption of *Penaeus vannamei*, Boone, 1931. *J. Aqua. Trop.* **11**, 59-65.
McGraw, I. J. (2007). The interactive effects of exercise and feeding on oxygen uptake activity levels, and gastric processing in the grateful crab *Cancer gracilis*. *Physiol. Biochem. Zool.* **80**, 335-343.
McMahon, B. R. (2001). Respiratory and circulatory compensation to hypoxia in crustaceans. *Respir. Physiol.* **128**, 349-364.
Mente, E., Legeay, A., Houlihan, D. F. and Massabuau, J.-C. (2003). Influence of oxygen partial pressures on protein synthesis in feeding crabs. *Am. J. Physiol.* **284**, R500-R510.
Meyer, R. A. (1988). A linear model of muscle respiration explains monoexponential phosphocreatine changes. *Am. J. Physiol.* **254**, C548-C553.
Milligan, C. L., Walsh, P. J., Booth, C. E. and McDonald, M. J. (1989). Intracellular acid-base regulation during recovery from locomotor activity in the blue crab *Callinectes sapidus*. *Physiol. Zool.* **62**, 813-825.
Morris, S. and Adamczewska, A. M. (2002). Utilisation of glycogen, ATP and arginine phosphate in exercise and recovery in terrestrial red crabs, *Gecarcoidea natalis*. *Comp. Biochem. Physiol. A.* **133**, 813-825.
Nyack, A. C., Locke, B. R., Valencia, A., Dillaman, R. M. and Kinsey, S. T. (2007). Scaling of post-contractile phosphocreatine recovery in fish white muscle: effect of intracellular diffusion. *Am. J. Physiol.* **292**, R1-R12.
Onnen, T. and Zebe, E. (1983). Energy metabolism on the tail muscles of the shrimp *Crangon crangon* during work and subsequent recovery. *Comp. Biochem. Physiol.* **74A**, 833-838.
Raffin, J. P., Thebault, M. T. and Le Gall, J. Y. (1988). Changes in phosphometabolites and intracellular pH in the tail muscle of the prawn *Palaemon serratus* as shown *in vivo* ^{31}P-NMR. *J. Comp. Physiol. B.* **158**, 223-228.
Richards, J. G., Heigenhauser, G. J. F. and Wood, C. M. (2003). Exercise and recovery metabolism in the pacific spiny dogfish (*Squalus acanthias*). *J. Comp. Physiol. B.* **173**, 463-474.
Russell, B., Motlagh, D. and Ashley, W. (2000). Form follows function: how muscle shape is regulated by work. *J. Appl. Phys.* **88**, 1127-1132.
Schmidt-Nielsen, K. (1984). Problems of size and scale. In *Scaling: Why is Animal Size So Important?* pp. 17-20. Cambridge: Cambridge University Press.
Somero, G. N. and Childress, J. J. (1990). Scaling of ATP-supplying enzymes, myofibrillar proteins and buffering capacity in fish muscle: relationship to locomotory habit. *J. Exp. Biol.* **149**, 319-333.
Taylor, E. W. (1982). Control and co-ordination of ventilation and circulation in crustaceans: responses to hypoxia and exercise. *J. Exp. Biol.* **100**, 289-319.
Villareal, H. and Ocampo, L. (1993). Effect of size and temperature on the oxygen consumption of the brown shrimp *Penaeus californiensis* (Holmes, 1900). *Comp. Biochem. Physiol.* **106A**, 97-101.
Walsh, P. J. and Henry, R. P. (1990). Activities of metabolite enzymes in the deep-water crabs *Chaceon fenneri* and *C. quinquedens* and the shallow-water crab *Callinectes sapidus*. *Mar. Biol.* **106**, 343-346.
Wang, Y., Heigenhauser, G. J. F. and Wood, C. M. (1994). Integrated responses to exhaustive and recovery in rainbow trout white muscle: Acid-base, phosphogen, carbohydrate, lipid, ammonia, fluid volume and electrolyte metabolism. *J. Exp. Biol.* **195**, 227-258.
Wells, R. M. G., Lu, J., Hickey, A. J. R. and Jeffs, A. G. (2001). Ontogenetic changes in enzyme activities associated with energy production in the spiny lobster, *Jasus edwardsii*. *Comp. Biochem. Physiol. B.* **130**, 339-347.
Winget, R. R. (1969). Oxygen consumption and respiratory energetics in the spiny lobster, *Panulirus interruptus* (Randall). *Biol. Bull.* **136**, 301-312.
Zoutendyk, P. (1989). Oxygen consumption by the cape rock lobster *Jasus lalandii*. *S. Afr. J. Mar. Sci.* **8**, 219-230.